ADVANCED MATERIALS INTERFACES
www.advmatinterfaces.de

Membrane-Mediated Self-Organization of Rod-Like DNA Origami on Supported Lipid Bilayers

Alena Khmelinskaia, Henri G. Franquelim, Renukka Yaadav, Eugene P. Petrov, and Petra Schwille**

Organization of elongated particles into ordered phases on 2D surfaces and interfaces has been extensively studied during the last decades both theoretically and experimentally. For mutually repulsive particles on solid nondeformable substrates, the process is controlled only by the aspect ratio and the surface density of the adsorbed particles. The local elastic response of soft substrates to particle adhesion can drastically change the collective behavior of adsorbed rod-like particles resulting in their self-organization via substrate-mediated interparticle attraction. Here, high-speed atomic force microscopy is used to study the organization of DNA origami particles on locally responsive supported lipid bilayers (SLBs) in comparison with that on nondeformable solid mica surfaces. At high surface coverage, the aspect ratio-dependent anisotropic phases expected for densely packed particles are observed. At intermediate and low surface densities, however, a drastically different phenomenology is observed: surprisingly strong surface-mediated interparticle attraction of DNA origami particles is found on SLBs resulting in their self-organization compared to their purely repulsive interaction on a mica surface. The formation of organized aggregates of elongated DNA origami particles on SLBs is explained by exceptionally strong nanoparticle adhesion to the membrane that responds with a local deformation in spite of the presence of the solid support.

1. Introduction

The organization of lipid membranes and in particular their interaction with macromolecules and colloids has been an exciting subject of investigation across different fields, from soft-matter physics to biomedical research. Indeed, the development of novel materials, carriers, and bioactive molecules (e.g., drugs, nanoparticles, and polymers) often requires a thorough investigation of the interactions, penetration, and toxicity of these molecules on biological or model lipid membranes.[1–5] On one hand, the size, shape, and strength of the membrane interaction of the particles of interest determine their organization on the lipid membrane.[6–9] On the other hand, membrane biophysical properties and shape depend on the membrane interaction with these particles: in particular, membrane protein organization has been proposed to influence the mechanics of lipid membranes,[10,11] viral infection is determined by the interaction of viruses with cellular membranes[12,13] and the wrapping and uptake of nanoparticles influences their delivery yield.[3]

Thus, from a physicochemical perspective, understanding the general interaction mechanisms of particles of different shapes and properties on biorelevant surfaces/interfaces, such as lipid membranes, is of great significance. Notably, several theoretical studies have predicted membrane-mediated self-organization of rigid rod-like particles.[14–22] However, studies of membrane-mediated organization of rod-like particles have been scarce. The first experimental evidence of this phenomenon has been the observation of tip-to-tip linear chain aggregates formed by rod-like fd virus particles electrostatically bound to a low-tension free-standing cationic lipid membrane.[23] More recently, DNA origami needles have been observed to organize in a parallel fashion or form aster-like structures after adsorption to free-standing cationic lipid membranes.[24]

Henceforth, to better understand the role of lipid membranes for the lateral self-organization of rigid colloidal particles, we set out to study the dynamic behavior of ensembles of rod-like DNA nanostructures of aspect ratio 7 (AR7)[25] (Figures S1 and S4, Supporting Information) adsorbed through Mg^{2+}-mediated electrostatic interactions on the solid mica surface and more elastically responsive 1,2-distearoyl-*sn*-glycero-3-phosphocholine (DSPC)

A. Khmelinskaia,[+] H. G. Franquelim, R. Yaadav,[++] E. P. Petrov, P. Schwille
Max Planck Institute of Biochemistry
Am Klopferspitz 18, 82152 Martinsried, Germany
E-mail: schwille@biochem.mpg.de
E. P. Petrov
Physikalisch-Technische Bundesanstalt
Abbestraße 2-12, 10587 Berlin, Germany
E-mail: eugene.petrov@ptb.de
The ORCID identification number(s) for the author(s) of this article can be found under https://doi.org/10.1002/admi.202101094.

[+]Present address: Life and Medical Sciences Institute, Chemical Biology, University of Bonn, Gerhard-Domagk-Straße 1, 53121 Bonn, Germany
[++]Present address: Department of Chemistry, Ludwig Maximilian University of Munich, Butenandtstr. 5-13, 81377 Munich, Germany

DOI: 10.1002/admi.202101094

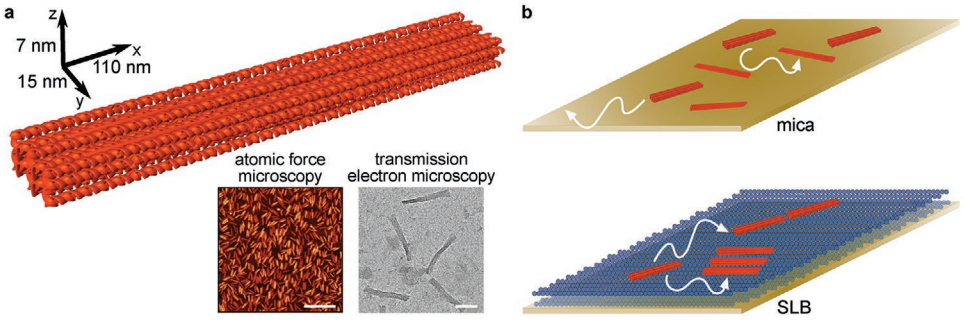

Figure 1. Schematic representation of the experimental setup. a) Model of DNA origami nanostructure AR7 of dimensions 7 nm × 15 nm × 110 nm. Atomic force microscopy (scale bar: 200 nm) and transmission electron microscopy (scale bar: 50 nm) images confirm the correct folding of the nanostructure into rods. b) DNA origami AR7 particles adsorbed on mica (top panel) or an SLB (bottom panel) and exhibiting translational and orientational dynamics in 2D, which can be observed using HSAFM. Higher order organization is expected to occur on SLBs, but not on mica.

supported lipid bilayers (SLBs) using high speed atomic force microscopy (HSAFM) (**Figure 1**). In this experimental approach, while the DNA origami technology allowed us to produce a monodisperse set of particles with a high yield,[26] the use of gel-phase DSPC membranes in combination with HSAFM[27] enabled us to track the diffusion and organization of individual particles even at low membrane densities.

2. Results

2.1. Particles Show Purely Repulsive Interactions on a Rigid Mica Surface

On the solid mica surface, DNA origami rods behave as independent hard particles exhibiting translational and rotational Brownian motion (**Figure 2**; Movies S1–S3, Supporting Information). At low particle densities, when the particle density does not affect the particle motion, free diffusion of the particles is observed. At higher surface densities, although the translational and rotational Brownian motion is suppressed due to particle crowding, no evidence of particle attraction and aggregate formation is found, suggesting purely repulsive interactions between DNA origami particles adsorbed on mica. Indeed, the Debye length under the conditions of this experiment is ≈0.7 nm, and thus, soluble charge-mediated particle attraction will only occur at very short length scales.

It has been theoretically predicted[28–31] and experimentally confirmed[32,33] that the organization of rod-like particles depends on their surface density. In particular, the isotropic phase observed at low surface densities transforms into an ordered phase upon increasing the density. For hard rectangles of aspect ratio 7, the isotropic–anisotropic transition is predicted to occur at reduced surface densities $\rho = \sigma L^2 \approx 3$–5, where σ is the particle surface density, and L is the rod length.[29,34,35] In agreement with the expectations, at relatively high densities ($\rho \approx 2.4$), although a certain degree of orientational anisotropy is attained as a result of crowding in the dense ensemble of mica-adsorbed DNA rods, the system still did not undergo a transition into a smectic phase (Figure 2c). Nonetheless, at a reduced surface density of $\rho \approx 2.9$, the particles form a quasi-smectic phase, as additionally confirmed by the spatial frequency spectrum (Figure 2d).

2.2. Membrane-Mediated Attractive Interactions Result in Particle Self-Organization

On SLBs, at low surface densities, ($\sigma \approx 2$–$3\ \mu m^{-2}$, $\rho \approx 0.02$–0.04) (**Figure 3**a; Movie S4, Supporting Information), the adsorbed DNA origami rods exhibited translational and orientational Brownian motion and showed the dynamics and organization generally similar to that observed for mica at similar surface densities (Figure 2a). In contrast to mica-adsorbed particles, however, a number of DNA nanoneedles adhering to the SLB exhibited a pronounced tip-to-tip attraction and formed stable linear chain aggregates (Figure 3a).

On the other hand, at higher surface densities, the organization of the nanostructures on the SLB was found to be strikingly different from that observed on mica. On SLBs, at surface densities in the regime $\sigma > 30\ \mu m^{-2}$ ($\rho > 0.4$), the nanostructures show a clear tendency of clustering and forming higher order aggregates. At intermediate surface densities of $\sigma \approx 30$–$50\ \mu m^{-2}$ ($\rho \approx 0.4$–0.6) both tip-to-tip and side-by-side attraction of DNA origami rods is observed (Figure 3b; Movie S5, Supporting Information). At high surface densities ($\sigma \approx 100$–$200\ \mu m^{-2}$, $\rho \approx 1.2$–2.4), interactions are clearly dominated by the side-by-side attraction (Figure 3c; Movie S6, Supporting Information), which results in anisotropic organization of SLB-adsorbed DNA origami rods into side-by-side bands. At an even higher surface density ($\sigma \approx 260\ \mu m^{-2}$, $\rho \approx 3.2$), when the membrane appears to be fully covered, the particles form a quasi-smectic phase (Figure 3d), just as observed on mica (cf. Figure 2d).

2.3. The Anisotropic Phase Formed at High Surface Density Depends on the Aspect Ratio

Our experimental setup further allows us to study anisotropic phases formed by particles of various aspect ratios, when deposited at high surface densities on membranes, under conditions where diffusion is strongly suppressed (Note S1, Supporting Information). To cover a range of shapes, two additional DNA origami nanostructures of aspect ratios 1 and 22 (AR1 and AR22, respectively) were designed (Figures S2–S4, Supporting Information) and the organization of the three nanostructures (including AR7) on DOPC/DSPC/Chol 2:2:1 SLBs exhibiting

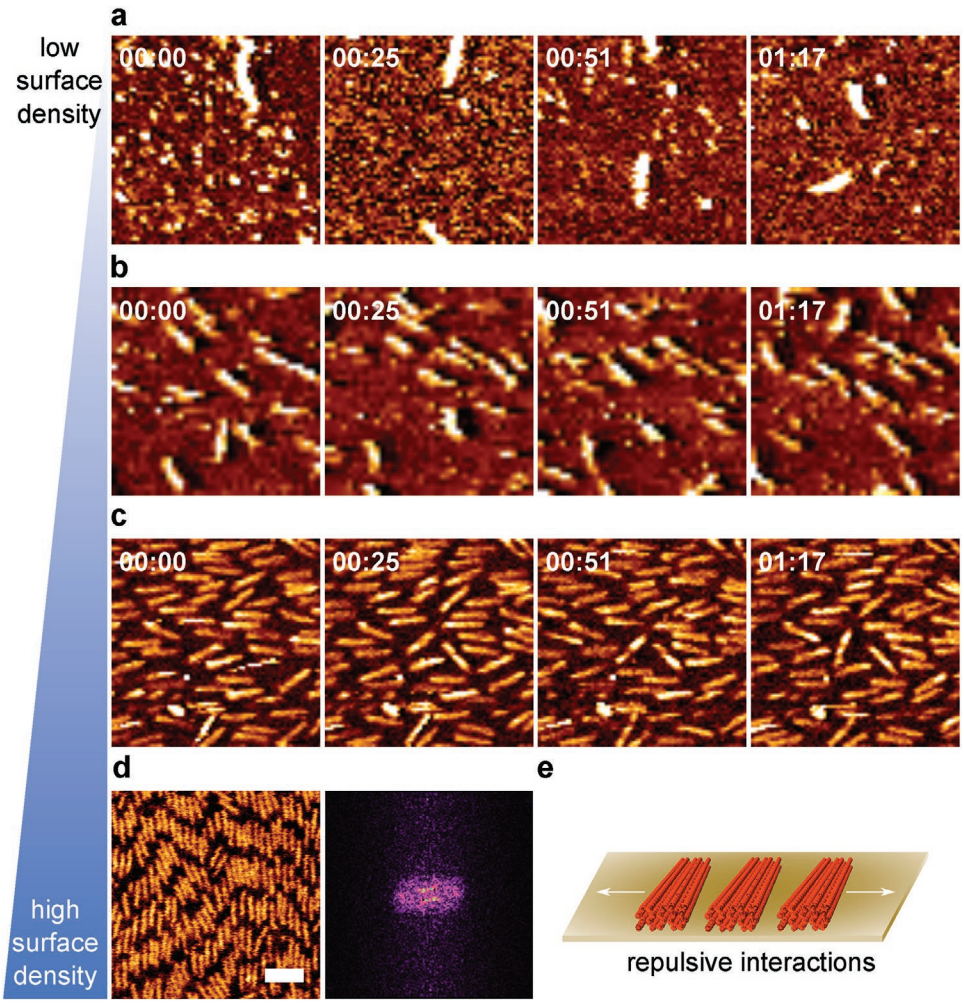

Figure 2. DNA nanostructures show purely repulsive interactions on a rigid surface. HSAFM images of DNA nanostructure AR7 diffusing on a mica surface at different surface densities: a) low ($\sigma \approx$ 2–3 μm^{-2}, $\rho \approx$ 0.02–0.04), b) intermediate ($\sigma \approx$ 30–50 μm^{-2}, $\rho \approx$ 0.4–0.6), and c,d) high ($\sigma \approx$ 200 μm^{-2}, $\rho \approx$ 2.4, and $\sigma \approx$ 240 μm^{-2}, $\rho \approx$ 2.9, respectively) surface area coverage. Snapshots in time are shown for each condition, except for panel (d), which shows very slow dynamics. The spatial frequency spectrum in panel (d) corresponds to the whole area shown. All experiments are performed at 16 mM $MgCl_2$ and 150 mM NaCl. Scale bar: 150 nm. e) Schematic representation of the interactions governing particle organization on a mica surface.

phase separation (Figure S5, Supporting Information) was studied using HSAFM (here DOPC and Chol denote 1,2-dioleoyl-*sn*-glycero-3-phosphocholine and cholesterol, respectively). This modified experimental setup allowed us to more readily achieve high surface densities at which anisotropic phases form, by local confinement of particles to membrane domains of a specific type (for details, see the Experimental Section).

For DNA nanoparticles of three different aspect ratios, anisotropic phases were observed at high surface densities, similar to what has been previously observed on mica.[33] Generally, for elongated particles three different phases (isotropic, nematic, and smectic) can be observed, which transform into one another upon an increase in the surface density and variation of the aspect ratio. Based on the theoretically predicted phase diagram for rod-like particles in 2D, a nematic phase is expected to form at high surface densities of particles with the aspect ratio in excess of 7, which, upon a further increase in the surface density, is followed by formation of a smectic phase.[29] Indeed, while for AR22, we could observe both a nematic phase (**Figure 4**a), in which particles orient directionally, and, at higher densities, a smectic phase (Figure 4b) characterized by both the directional and positional order, for less elongated AR7 particles only a smectic phase could be observed (Figure 4c). In contrast, the seemingly simple case of Brownian squares (particles of aspect ratio 1) was found to show an unexpectedly rich succession of phases depending on the packing density.[36–38] At high densities square-shaped particles have been shown to freeze into the translationally and orientationally ordered square crystalline phase with suppressed translational diffusion.[38] This is what we indeed observe in our experiments with square-shaped DNA nanoparticles AR1 (Figure 4d).

3. Discussion

The 2D isotropic–anisotropic phase transition of particles has been theoretically predicted to take place at different surface densities depending on the particle aspect ratio.[28–31,37,39] In

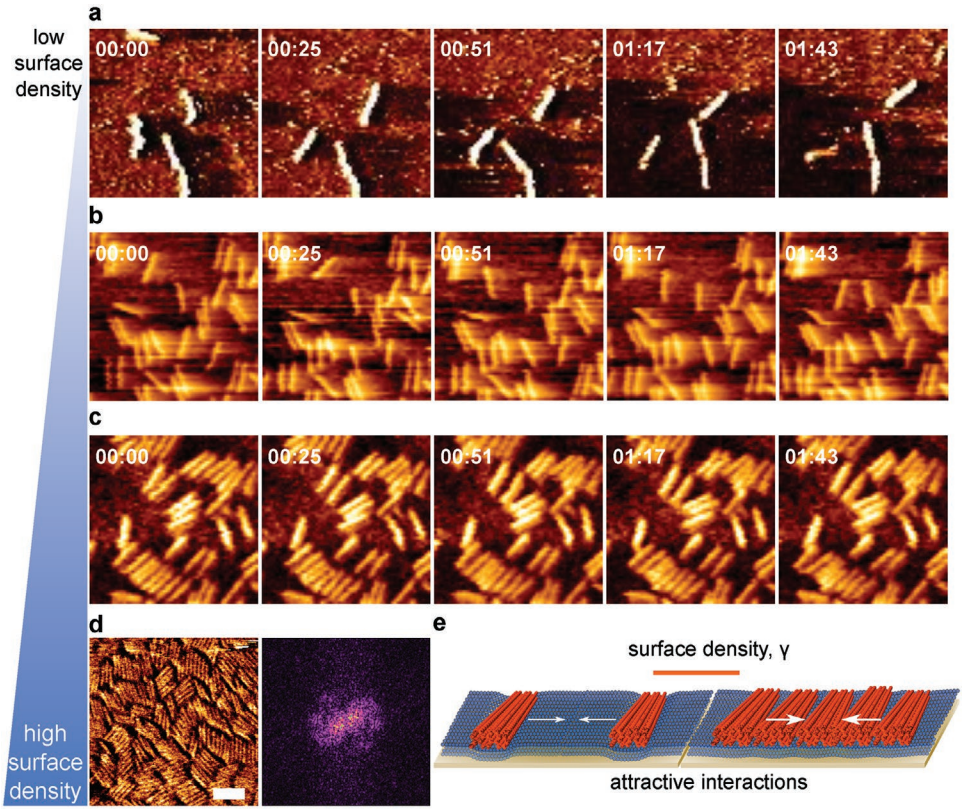

Figure 3. DNA nanostructures show tip-to-tip and side-by-side attraction on SLBs. HSAFM images of DNA nanostructure AR7 diffusing on DSPC SLBs at different surface densities: a) low ($\sigma \approx$ 2–3 μm^{-2}, $\rho \approx$ 0.02–0.04), b) intermediate ($\sigma \approx$ 30–50 μm^{-2}, $\rho \approx$ 0.4–0.6), and c,d) high ($\sigma \approx$ 100–200 μm^{-2}, $\rho \approx$ 1.2–2.4 and $\sigma \approx$ 260 μm^{-2}, $\rho \approx$ 3.2, correspondingly). Snapshots in time are shown for each condition, except for panel (d), which shows very slow dynamics. The spatial frequency spectrum in panel (d) corresponds to the whole area shown. All experiments were performed at 20 mM $MgCl_2$. Scale bar: 150 nm. e) Schematic representation of higher order organization of DNA nanostructures at higher surface densities due to increased membrane tension.

most previous experiments[32,36,40–44] such isotropic–anisotropic phase transitions have been observed by varying the surface density of particles of a fixed aspect ratio (1 to 70), with the exception of a study that employed DNA origami particles with various shapes.[33] Furthermore, to the best of our knowledge, to date no experimental study has been carried out where isotropic–anisotropic phase transitions of particles of different aspect ratios in 2D were observed for particles with the same physicochemical properties under identical conditions and on a biologically relevant surface. This again demonstrates that,

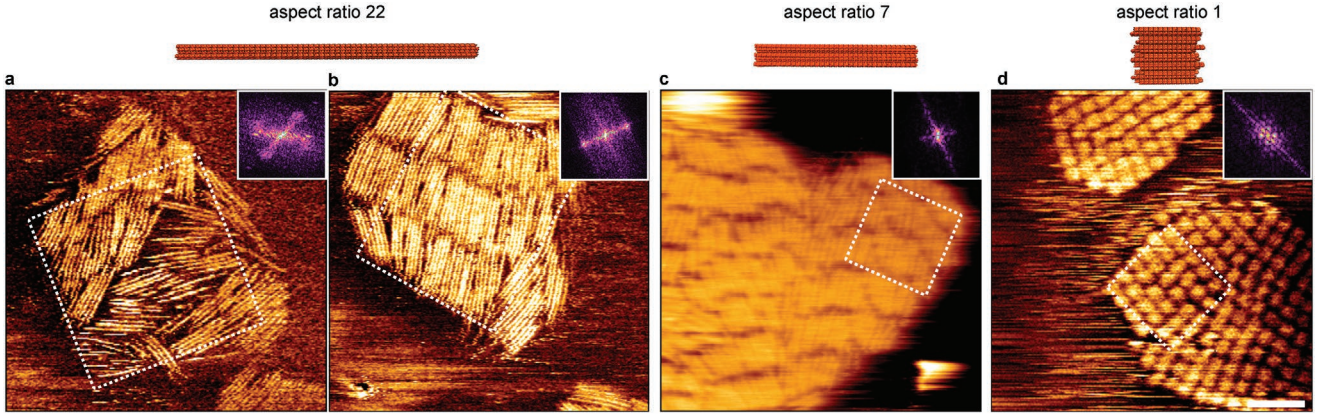

Figure 4. Anisotropic phases formed by DNA nanostructures at high surface densities. HSAFM images of a) nematic and b) smectic phases formed by DNA nanostructures of aspect ratio 22, c) smectic phase formed by DNA nanostructure of aspect ratio 7, and d) square crystalline phase formed by DNA nanostructure of aspect ratio 1 on DOPC:DSPC:Chol (2:2:1) SLBs. The spatial frequency spectra of the square areas marked by the dotted line are shown in the corresponding insets for illustration purposes. Scale bar: 200 nm.

as it has been previously suggested,[32] DNA origami nanotechnology is a perfect tool for a comprehensive study of colloidal organization on surfaces that allows one to cover a wide range of aspect ratios (for elongated particles) and, generally, address other particle geometries, as DNA origami structures of virtually any shape can be produced with high yield.[45] Moreover, we have introduced an experimental setup that allows the conduction of such rigorous studies on lipid membranes.

The theory and simulations predict that the local deformation of elastic surfaces upon adhesion of rod-like particles should result in attractive interactions between the particles. In particular, for an elastic lipid bilayer with a given bending rigidity κ, the character of these interactions should depend on the membrane tension γ:[17,19,21,22,46] at low membrane tension γ, tip-to-tip attraction is expected to dominate, while at higher γ, side-by-side attraction becomes more favorable. For an elastic but essentially nonstretchable lipid membrane, electrostatic binding of a nanoparticle locally deforms the membrane as a result of its strong adhesion, and leads to an increase in the membrane tension (for illustration, see schematic in Figure 3e). Thus, with an increase in the number of bound nanoparticles, the membrane tension grows, and consequently the preference is expected to shift gradually from tip-to-tip to side-by-side attraction. Our observations of prevalent tip-to-tip attraction at low particle densities and side-by-side attraction at high particle densities perfectly agree with this line of reasoning.

Now let us verify whether the parameters of our experimental system are consistent with the proposed interaction mechanism. The characteristic length scale at which membrane-mediated attraction of membrane-bound nanoparticles takes place can be estimated as $l \sim \sqrt{\kappa/\gamma}$.[46] From our observation of the formation of stable interactions at the intermediate and high density regimes, we estimate that $l \approx 100$ nm, at least two orders of magnitude larger than the Debye screening length under the conditions of the experiment (≈1.2 nm). For a lipid well below its phase transition temperature T_m, such as DSPC at 20 °C (T_m = 55 °C), the bending rigidity κ is expected to be $\approx 10^3\ k_B T$.[47] Indeed, under our experimental conditions, force spectroscopy experiments yield $\kappa \approx 500\ k_B T$ (Note S1, Supporting Information). This gives a reasonable estimate of the membrane tension $\gamma \approx 10^{-4}$–10^{-3} N m^{-1}, at least one order of magnitude below the typical membrane rupture tension (10^{-2} N m^{-1}).[48] Thus, the suggested mechanism of membrane-mediated interactions generally agrees with the mechanical properties of the lipid bilayer. Importantly, although SLBs do not allow for high-magnitude deformations on a solid support, nanometer-scale deformations are possible, due to the presence of a hydration layer between the support surface and the phospholipid headgroups (Note S1, Supporting Information).[49–51]

Interestingly, while membrane-mediated interactions of elongated colloidal particles have been previously observed on free-standing lipid bilayers,[23,24] no evidence of membrane-mediated interactions has been reported for macromolecules and colloidal particles adsorbed on SLBs.[23,52–55] A potential reason for that could be that all these experiments were carried out using cationic lipid bilayers strongly adhering to the oppositely charged mica surface via electrostatic attraction. In the present study, however, the zwitterionic lipid bilayer was bound to the negatively charged mica surface indirectly, via Mg^{2+} ions. Thus, the reason for the drastically different phenomenology can be due to the considerably looser binding of the bilayer to the solid substrate in our experiments.

At fixed membrane rigidity and tension, the strength of the interaction between the elastic membrane and the adsorbed nanoparticle plays a crucial role in the type of interactions observed.[22,23,46] In the previous experimental studies,[23,24,52–55] the membrane binding was mediated through electrostatic interactions of negatively charged macromolecules and colloids with positively charged lipids, the amount of which typically never exceeded a few percent, while here, the membrane is covered with Mg^{2+} cations that coordinate with the phosphate groups of the saturated phospholipids.[56] In other words, each lipid of the highly packed lipid bilayer bears a net positive charge. The positive charge density in solution of the lipid mixture used in this study in the respective buffer conditions is the same order of magnitude as those of the lipid mixtures used in previous studies (Note S2, Supporting Information). Nonetheless, using a previously described approach,[57] the linear charge density of our DNA nanostructure AR7 is estimated to be 16 e$^-$ nm^{-1} and is higher than that of previously studied particles[23,54,55] (2 e$^-$ nm^{-1} for dsDNA,[58] 10 e$^-$ nm^{-1} for fd bacteriophage particles[59]). This results in a stronger interaction of the lipid bilayer with the DNA nanoparticles in comparison with the macromolecules and colloids used in previous studies, and thus allows one to achieve higher surface tension and observe a range of self-organization regimes, which so far has been only achieved in vesicles fully composed of cationic lipids.[24]

Although some experiments on interactions of macromolecules with lipid membranes in the gel phase have been carried out previously,[55] these did not allow one to conclude on the existence of membrane-mediated interactions on gel-phase membranes. In these experiments, negatively charged macromolecules were directly electrostatically bound to cationic headgroups of lipid molecules residing in the bilayer. As a result, the transition of the membrane into the gel phase that is characterized by an extremely low lipid mobility,[60] automatically leads to freezing of the motion of the adsorbed macromolecules and thus precludes observation of membrane-mediated interactions. Importantly, the present experimental setting, although also based on gel-phase bilayers, employs an indirect binding of the negatively charged DNA origami particles via Mg^{2+} ions to zwitterionic lipids, thus uncoupling their translational dynamics from that of the lipid molecules in the underlying bilayer, and allows one to observe membrane-mediated interactions on the gel-phase lipid bilayer.

While varying the type of cations mediating the DNA nanoparticle interaction with the lipid bilayer may influence to some extent the organization and dynamics of lipid membranes (e.g., refs. [61–64]) as well as DNA nanostructures,[65] we expect that the phenomena described above will remain unaffected, as only the rate of equilibration and assembly/disassembly kinetics of the particle aggregates would be influenced by changes in the translational diffusion rates.

In recent years, there has been an increased interest in the interplay of cellular lipid membranes with membrane proteins.[66] The shapes and morphology of highly curved lipid membrane structures in living cells are controlled and

modulated by several types of scaffolding proteins,[67] such as the BAR domain superfamily.[68] The general common feature of these proteins is their strongly elongated banana shape with the membrane-binding motif typically located on the concave (very rarely on the convex) side of the molecule. As a result, these proteins exhibiting a membrane-curving ability possess a strongly elongated rod shape in the membrane plane. It has been suggested that self-organization of elongated protein molecules on the nanoscale into nematic domains enhances the effect of individual protein molecules and generates an anisotropic spontaneous curvature of the protein-decorated membrane.[16,69–71] Thus, in spite of the different chemical structure of these proteins, their membrane-bending effect largely relies on one and the same physical mechanism, which is governed by their collective behavior. Therefore, the basic properties of the phenomenon can be understood using a model synthetic biology-inspired approach[72] with building blocks artificially created to mimic the essential physical properties of the part of the living system under consideration, such as the one employed in this study.

4. Conclusion

To conclude, our high-speed atomic force experiments on DNA origami rods on mica and SLBs allowed us to observe both tip-to-tip and side-by-side membrane-mediated interactions of rod-like nanoparticles on gel-phase SLBs and further demonstrated the qualitatively different behavior of elongated particles on rigid and mechanically responsive elastic surfaces. Our experimental setup, by combining the power of HSAFM with the structural versatility of DNA origami, opens the door to further explorations of the membrane-mediated interparticle-interaction space.

5. Experimental Section

DNA Origami Folding and Purification: DNA origami nanostructures consisting of a 20-, 52-, and 12-helix bundle with hexagonal lattice based on the M13mp18 7429-nucleotide long scaffold plasmid (p7429) was designed using CaDNAno[73] (Figures S1–S3, Supporting Information). To avoid stacking interactions between monomers of each structure,[74,75] the oligonucleotides at the tips of each structure had been extended with two/six adenines. Additionally, the DNA origami nanostructure of aspect ratio 1 had been designed with irregular helix length to reduce the number of possible stacking interactions due to shape complementarity.[75] High purity salt free (HPSF) purified staple oligonucleotides needed for origami folding were purchased from Eurofins MWG Operon (Ebersberg, Germany), and single-stranded M13mp18 scaffold DNA was supplied by Bayou Biolabs (Metairie, LA, USA). DNA origami nanostructures were folded and purified in folding buffer (FOB) containing 5 mM Tris-HCl, 1 mM ethylenediaminetetraacetic acid (EDTA), and 20 mM $MgCl_2$, pH 8.0 as previously described.[25,76]

Transmission Electron Microscopy (TEM): To confirm the folding of the DNA origami nanostructures (Figure 1a; Figure S4b, Supporting Information), negative-stain TEM imaging was performed on a CM120 BioTWIN (FEI/Philips, Hillsboro, Oregon, USA), with a LaB6 filament operated at 120 kV. Images were recorded with a MegaView III camera (Soft Imaging System GmbH, Münster, Germany). Typically, 3 µL of folded, purified, and diluted (1/10 in FOB buffer) DNA origami nanostructures were adsorbed on glow-discharged formvar-supported carbon coated Cu300 grids (Plano GmbH, Wetzlar, Germany) and stained using a 2% aqueous uranyl formate solution containing 25 mM sodium hydroxide.[76] Further image analysis was performed using the ImageJ software (http://rsb.info.nih.gov/ij/).[77]

Agarose Gel Electrophoresis: The folding quality of the DNA origami nanostructures AR1, AR7, and AR22 was investigated through agarose gel electrophoresis (Figure S4a, Supporting Information), as described elsewhere.[76] Briefly, the assembled DNA origami structures were loaded into 2% agarose gels containing 0.5× TBE buffer (40 mM Tris-Cl, 45 mM boric acid, and 1 mM EDTA, pH 8.3) and 11 mM $MgCl_2$. The GeneRuler Express DNA ladder from ThermoFischer Scientific was used. Electrophoresis was performed at 70 V for ≈2 h, in an ice water bath. SYBR Safe for DNA staining (10 µL of stock solution) was directly added to the gels prior to electrophoresis. At the end of electrophoresis, gels were scanned using a Peqlab E-BOX VX2 Gel Documentation System (VWR International GmbH, Erlangen, Germany).

SLB Preparation: DSPC, DOPC, and Chol were purchased from Avanti Polar Lipids (Alabaster, AL, USA). Pure DSPC and phase separated DOPC/DSPC/Chol (2:2:1)[78] SLBs were formed at 60 °C via fusion of small unilamellar vesicles (SUVs) deposited in FOB buffer on top of freshly cleaved mica, following the general protocol described elsewhere.[79] After a washing step, the SLBs were slowly cooled down to room temperature (20 °C) in order to reduce the occurrence of membrane defects. The use of gel-phase DSPC membranes not only enhanced the interaction of DNA nanostructures with the membrane due to the higher charge density of the membrane when compared to less ordered phases,[80–84] but also slowed down the overall diffusion of DNA nanostructures thus facilitating the particle imaging and tracking. On DOPC/DSPC/Chol (2:2:1) lipid bilayers showing coexistence of the liquid-ordered (l_o) and liquid-disordered (l_d) phases (Figure S5, Supporting Information), DNA nanostructures adsorbed to lipid membranes via Mg^{2+}-mediated electrostatic interactions preferentially bind to the l_o phase.[80–84] This reduces the amount of the DNA origami material necessary to achieve the range of surface densities at which anisotropic phases of membrane-adsorbed DNA origami particles are formed. Moreover, DNA nanoparticles can cross the l_o–l_d interface back and forth[82–84] thus allowing for particle reorganization—and hence reaching the equilibrium state of the system—even at high surface densities.

Atomic Force Microscopy: Different volumes of solutions of purified DNA nanostructures were deposited on freshly cleaved mica or SLBs through electrostatic interactions mediated by $MgCl_2$. In FOB buffer, DNA nanostructures were completely immobilized on mica while freely diffusing on SLBs (e.g., refs. [82–85]). To allow the diffusion of DNA nanostructures on mica, FOB buffer was doped with NaCl to reach 10:1 proportionality relatively to $MgCl_2$,[33,65] with a final buffer composition 5 mM Tris-HCl, 1 mM EDTA, 16 mM $MgCl_2$, and 150 mM NaCl, pH 8.0. The addition of monovalent ions, i.e., Na^+, weakens the interactions between the DNA origami nanostructures and the support through partial replacement of Mg^{2+} ions.[86]

HSAFM in the tapping mode was performed with the Nanowizard Ultra module (JPK Instruments, Germany), using USC-F0.3-k0.3 ultrashort cantilevers from Nanoworld (Neuchâtel, Switzerland) with typical stiffness of 0.3 N m^{-1}. The cantilever oscillation was tuned to a frequency of 100–150 kHz and the amplitude was kept below 10 nm. Scan rate was set to 25–150 Hz. Typically, 1 × 1 µm or 2 × 2 µm images with 256 × 256 pixel were acquired. All measurements were performed at room temperature (20 °C). The force applied on the sample was minimized by continuously adjusting the set point and gain during imaging. Height, error, deflection, and phase-shift signals were recorded and images were line-fitted as required. Data were analyzed using JPK data processing software Version 5.1.4 (JPK Instruments, Germany), Gwyddion Version 2.45 (Czech Metrology Institute), and ImageJ (http://rsb.info.nih.gov/ij/).[77]

Supporting Information

Supporting Information is available from the Wiley Online Library or from the author.

Acknowledgements

This work was supported by the collaborative research project SFB 863 of the Deutsche Forschungsgemeinschaft. A.K. acknowledges the support of the Graduate School of Quantitative Biosciences Munich; R.Y. acknowledges the financial support by the Deutsche Forschungsgemeinschaft within the SFB 1032; H.G.F. acknowledges the receipt of a Humboldt Research Fellowship (PTG/1152511/STP); E.P.P. acknowledges the financial support by the Deutsche Forschungsgemeinschaft within the SFB 1032 TP B01 and A09. Further support was given by the Max Planck Society to P.S. The authors acknowledge the support by the Center for NanoScience Munich. Correction added on 24 January 2022, after first online publication: Petra Schwille was designated as corresponding author.

Open access funding enabled and organized by Projekt DEAL.

Conflict of Interest

The authors declare no conflict of interest.

Data Availability Statement

The data that support the findings of this study are available from the corresponding author upon reasonable request.

Keywords

DNA origami, high-speed atomic force microscopy, membrane-mediated self-organization, supported lipid bilayers

Received: June 28, 2021
Revised: August 1, 2021
Published online: October 18, 2021

[1] C. Peetla, A. Stine, V. Labhasetwar, *Mol. Pharmaceutics* **2009**, *6*, 1264.
[2] A. M. Seddon, D. Casey, R. V. Law, A. Gee, R. H. Templer, O. Ces, *Chem. Soc. Rev.* **2009**, *38*, 2509.
[3] E. Alipour, D. Halverson, S. McWhirter, G. C. Walker, *Annu. Rev. Phys. Chem.* **2017**, *68*, 261.
[4] D. Bochicchio, E. Panizon, L. Monticelli, G. Rossi, *Sci. Rep.* **2017**, *7*, 6357.
[5] C. Contini, M. Schneemilch, S. Gaisford, N. Quirke, *J. Exp. Nanosci.* **2018**, *13*, 62.
[6] B. D. Chithrani, W. C. W. Chan, *Nano Lett.* **2007**, *7*, 1542.
[7] P. R. Leroueil, S. Hong, A. Mecke, J. R. Baker Jr., B. G. Orr, M. M. Banaszak Holl, *Acc. Chem. Res.* **2007**, *40*, 335.
[8] M. Werner, T. Auth, P. A. Beales, J. B. Fleury, F. Höök, H. Kress, R. C. Van Lehn, M. Müller, E. P. Petrov, L. Sarkisov, J.-U. Sommer, V. A. Baulin, *Biointerphases* **2018**, *13*, 028501.
[9] C. Contini, J. W. Hindley, T. J. Macdonald, J. D. Barritt, O. Ces, N. Quirke, *Commun. Chem.* **2020**, *3*, 130.
[10] Z. Shi, T. Baumgart, *Nat. Commun.* **2015**, *6*, 5974.
[11] A. Szuba, F. Bano, G. Castro-Linares, F. Iv, M. Mavrakis, R. P. Richter, A. Bertin, G. H. Koenderink, *eLife* **2021**, *10*, e63349.
[12] D. A. Marvin, M. F. Symmons, S. K. Straus, *Prog. Biophys. Mol. Biol.* **2014**, *114*, 80.
[13] Q. Zhang, F. Tian, F. Wang, Z. Guo, M. Cai, H. Xu, H. Wang, G. Yang, X. Shi, Y. Shan, Z. Cui, *ACS Nano* **2020**, *14*, 7046.
[14] P. G. Dommersnes, J.-B. Fournier, *Eur. Phys. J. B* **1999**, *12*, 9.
[15] X. Wen, D. Zhang, A. Chai, L. He, S. Ran, L. Zhang, *Soft Matter* **2012**, *8*, 6706.
[16] N. Ramakrishnan, P. B. Sunil Kumar, J. H. Ipsen, *Biophys. J.* **2013**, *104*, 1018.
[17] T. Yue, X. Wang, F. Huang, X. Zhang, *Nanoscale* **2013**, *5*, 9888.
[18] M. Simunovic, A. Srivastava, G. A. Voth, *Proc. Natl. Acad. Sci. USA* **2013**, *110*, 20396.
[19] M. Simunovic, G. A. Voth, *Nat. Commun.* **2015**, *6*, 7219.
[20] Y.-Y. Zhang, Y.-F. Hua, Z.-Y. Deng, *Chin. Phys. B* **2015**, *24*, 118202.
[21] A. D. Olinger, E. J. Spangler, P. B. S. Kumar, M. Laradji, *Faraday Discuss.* **2016**, *186*, 265.
[22] S. K. Ghosh, A. G. Cherstvy, E. P. Petrov, R. Metzler, *Soft Matter* **2016**, *12*, 7908.
[23] A. B. Petrova, C. Herold, E. P. Petrov, *Soft Matter* **2017**, *13*, 7172.
[24] S. E. Zuraw-Weston, M. Siavashpouri, M. E. Moustaka, T. Gerling, H. Dietz, S. Fraden, A. E. Ribbe, A. D. Dinsmore, *Langmuir* **2021**, *37*, 6219.
[25] A. Khmelinskaia, H. G. Franquelim, E. P. Petrov, P. Schwille, *J. Phys. D* **2016**, *49*, 194001.
[26] S. Dey, C. Fan, K. V. Gothelf, J. Li, C. Lin, L. Liu, N. Liu, M. A. D. Nijenhuis, B. Saccà, F. C. Simmel, H. Yan, P. Zhan, *Nat. Rev. Methods Primers* **2021**, *1*, 13.
[27] W. Cai, Z. Liu, Y. Chen, G. Shang, *Sci. Technol. Adv. Mater.* **2017**, *9*, 77.
[28] D. Frenkel, R. Eppenga, *Phys. Rev. A* **1985**, *31*, 1776.
[29] M. A. Bates, D. Frenkel, *J. Chem. Phys.* **2000**, *112*, 10034.
[30] M. D. Khandkar, M. Barma, *Phys. Rev. E* **2005**, *72*, 051717.
[31] R. L. C. Vink, *Eur. Phys. J. B* **2009**, *72*, 225.
[32] A. Czogalla, D. J. Kauert, R. Seidel, P. Schwille, E. P. Petrov, *Nano Lett.* **2015**, *15*, 649.
[33] A. A. Rafat, T. Pirzer, M. B. Scheible, A. Kostina, F. C. Simmel, *Angew. Chem., Int. Ed.* **2014**, *53*, 7665.
[34] Y. Martínez-Ratón, E. Velasco, L. Mederos, *J. Chem. Phys.* **2005**, *122*, 064903.
[35] C. E. Sitta, F. Smallenburg, R. Wittkowski, H. Löwen, *Phys. Chem. Chem. Phys.* **2018**, *20*, 5285.
[36] K. Zhao, R. Bruinsma, T. G. Mason, *Proc. Natl. Acad. Sci. USA* **2011**, *108*, 2684.
[37] C. Avendaño, F. A. Escobedo, *Soft Matter* **2012**, *8*, 4675.
[38] L. Walsh, N. Menon, *J. Stat. Mech.: Theory Exp.* **2016**, *2016*, 083302.
[39] W.-S. Xu, Y.-W. Li, Z.-Y. Sun, L.-J. An, *J. Chem. Phys.* **2013**, *139*, 024501.
[40] S. Kwan, F. Kim, J. Akana, P. Yang, *Chem. Commun.* **2001**, 447.
[41] F. Kim, S. Kwan, J. Akana, P. Yang, *J. Am. Chem. Soc.* **2001**, *123*, 4360.
[42] M. J. A. Hore, R. J. Composto, *ACS Nano* **2010**, *4*, 6941.
[43] Z. Zheng, Y. Han, *J. Chem. Phys.* **2010**, *133*, 124509.
[44] Z. Zheng, F. Wang, Y. Han, *Phys. Rev. Lett.* **2011**, *107*, 065702.
[45] M. R. Jones, N. C. Seeman, C. A. Mirkin, *Science* **2015**, *347*, 1260901.
[46] A. G. Cherstvy, E. P. Petrov, *Phys. Chem. Chem. Phys.* **2014**, *16*, 2020.
[47] R. Dimova, *Adv. Colloid Interface Sci.* **2014**, *208*, 225.
[48] E. Evans, V. Heinrich, F. Ludwig, W. Rawicz, *Biophys. J.* **2003**, *85*, 2342.
[49] S. J. Johnson, T. M. Bayerl, D. C. McDermott, G. W. Adam, A. R. Rennie, R. K. Thomas, E. Sackmann, *Biophys. J.* **1991**, *59*, 289.
[50] B. W. Koenig, S. Krueger, W. J. Orts, C. F. Majkrzak, N. F. Berk, J. V. Silverton, K. Gawrisch, *Langmuir* **1996**, *12*, 1343.
[51] T. V. Ratto, M. L. Longo, *Biophys. J.* **2002**, *83*, 3380.
[52] B. Maier, J. O. Rädler, *Phys. Rev. Lett.* **1999**, *82*, 1911.
[53] B. Maier, J. O. Rädler, *Macromolecules* **2000**, *33*, 7185.
[54] C. Herold, P. Schwille, E. P. Petrov, *Phys. Rev. Lett.* **2010**, *104*, 148102.
[55] C. Herold, P. Schwille, E. P. Petrov, *J. Phys. D* **2016**, *49*, 074001.
[56] L. J. Lis, W. T. Lis, V. A. Parsegian, R. P. Rand, *Biochemistry* **1981**, *20*, 1771.
[57] G. Bellot, M. A. McClintock, J. J. Chou, W. M. Shih, *Nat. Protoc.* **2013**, *8*, 755.

[58] Y. Zhang, H. Zhou, Z.-C. Ou-Yang, in *Biological Physics 2000* (Eds: V. Sa-yakanit, L. Matsson, H. Frauenfelder), World Scientific, Singapore **2001**, pp. 294–325.
[59] K. Zimmermann, H. Hagedorn, C. C. Heuck, M. Hinrichsen, H. Ludwig, *J. Biol. Chem.* **1986**, *261*, 1653.
[60] G. van Meer, D. R. Voelker, G. W. Feigenson, *Nat. Rev. Mol. Cell Biol.* **2008**, *9*, 112.
[61] R. A. Böckmann, A. Hac, T. Heimburg, H. Grubmüller, *Biophys. J.* **2003**, *85*, 1647.
[62] R. Vácha, S. W. I. Siu, M. Petrov, R. A. Böckmann, J. Barucha-Kraszewska, P. Jurkiewicz, M. Hof, M. L. Berkowitz, P. Jungwirth, *J. Phys. Chem. A* **2009**, *113*, 7235.
[63] M. Javanainen, A. Melcrová, A. Magarkar, P. Jurkiewicz, M. Hof, P. Jungwirth, H. Martinez-Seara, *Chem. Commun.* **2017**, *53*, 5380.
[64] S. M. Baumler, G. J. Blanchard, *Langmuir* **2017**, *33*, 2986.
[65] S. Woo, P. W. K. Rothemund, *Nat. Commun.* **2014**, *5*, 4889.
[66] H. T. McMahon, J. L. Gallop, *Nature* **2005**, *438*, 590.
[67] T. Baumgart, B. R. Capraro, C. Zhu, S. L. Das, *Annu. Rev. Phys. Chem.* **2011**, *62*, 483.
[68] A. Frost, V. M. Unger, P. De Camilli, *Cell* **2009**, *137*, 191.
[69] M. Simunovic, C. Mim, T. C. Marlovits, G. Resch, V. M. Unger, G. A. Voth, *Biophys. J.* **2013**, *105*, 711.
[70] H. Cui, C. Mim, F. X. Vázquez, E. Lyman, V. M. Unger, G. A. Voth, *Biophys. J.* **2013**, *104*, 404.
[71] R. Lipowsky, *Faraday Discuss.* **2013**, *161*, 305.
[72] P. Schwille, *Science* **2011**, *333*, 1252.
[73] S. M. Douglas, A. H. Marblestone, S. Teerapittayanon, A. Vazquez, G. M. Church, W. M. Shih, *Nucleic Acids Res.* **2009**, *37*, 5001.
[74] S. Woo, P. W. K. Rothemund, *Nat. Chem.* **2011**, *3*, 620.
[75] T. Gerling, K. F. Wagenbauer, A. M. Neuner, H. Dietz, *Science* **2015**, *347*, 1446.
[76] C. E. Castro, F. Kilchherr, D.-N. Kim, E. L. Shiao, T. Wauer, P. Wortmann, M. Bathe, H. Dietz, *Nat. Methods* **2011**, *8*, 221.
[77] J. Schindelin, C. T. Rueden, M. C. Hiner, K. W. Eliceiri, *Mol. Reprod. Dev.* **2015**, *82*, 518.
[78] G. W. Feigenson, *Nat. Chem. Biol.* **2006**, *2*, 560.
[79] S. Chiantia, N. Kahya, P. Schwille, *Langmuir* **2005**, *21*, 6317.
[80] M. Pisani, P. Bruni, G. Caracciolo, R. Caminiti, O. Francescangeli, *J. Phys. Chem. B* **2006**, *110*, 13203.
[81] A. Kato, A. Tsuji, M. Yanagisawa, D. Saeki, K. Juni, Y. Morimoto, K. Yoshikawa, *J. Phys. Chem. Lett.* **2010**, *1*, 3391.
[82] C. Dohno, S. Makishi, K. Nakatani, S. Contera, *Nanoscale* **2017**, *9*, 3051.
[83] N. Avakyan, J. W. Conway, H. F. Sleiman, *J. Am. Chem. Soc.* **2017**, *139*, 12027.
[84] Y. Sato, M. Endo, M. Morita, M. Takinoue, H. Sugiyama, S. Murata, S.-I. M. Nomura, Y. Suzuki, *Adv. Mater. Interfaces* **2018**, *5*, 1800437.
[85] Y. Suzuki, M. Endo, H. Sugiyama, *Nat. Commun.* **2015**, *6*, 8052.
[86] D. Pastré, O. Piétrement, S. Fusil, F. Landousy, J. Jeusset, M.-O. David, L. Hamon, E. L. Cam, A. Zozime, *Biophys. J.* **2003**, *85*, 2507.